Microscopic model for the ferroelectric field effect in oxide heterostructures

Shuai Dong,[1,2] Xiaotian Zhang,[3,4] Rong Yu,[5] J.-M. Liu,[2,6] and Elbio Dagotto[3,4]
[1]*Department of Physics, Southeast University, Nanjing 211189, China*
[2]*National Laboratory of Solid State Microstructures, Nanjing University, Nanjing 210093, China*
[3]*Department of Physics and Astronomy, University of Tennessee, Knoxville, Tennessee 37996, USA*
[4]*Materials Science and Technology Division, Oak Ridge National Laboratory, Oak Ridge, Tennessee 37831, USA*
[5]*Department of Physics and Astronomy, Rice University, Houston, Texas 77005, USA*
[6]*International Center for Materials Physics, Chinese Academy of Sciences, Shenyang 110016, China*
(Received 21 September 2011; published 14 October 2011)

A microscopic model Hamiltonian for the ferroelectric field effect is introduced for the study of oxide heterostructures with ferroelectric components. The long-range Coulomb interaction is incorporated as an electrostatic potential, solved self-consistently together with the charge distribution. A generic double-exchange system is used as the conducting channel, epitaxially attached to the ferroelectric gate. The observed ferroelectric screening effect, namely, the charge accumulation/depletion near the interface, is shown to drive interfacial phase transitions that give rise to robust magnetoelectric responses and bipolar resistive switching, in qualitative agreement with previous density functional theory calculations. The model can be easily adapted to other materials by modifying the Hamiltonian of the conducting channel, and it is useful in simulating ferroelectric field effect devices particularly those involving strongly correlated electronic components where *ab initio* techniques are difficult to apply.

DOI: 10.1103/PhysRevB.84.155117 PACS number(s): 85.30.Tv, 75.47.Lx, 77.80.−e, 85.75.Hh

I. INTRODUCTION

The research area known as oxide heterostructures continues attracting considerable attention of the condensed matter community due to the rich physical properties of its constituents, often involving strongly correlated electronic materials, and also for their broad potential in device applications.[1–4] Among these heterostructures, those involving ferroelectric (FE) and magnetic, or multiferroic, components are particularly interesting since they could be used in the next generation of transistors and nonvolatile memories.[5–7] From the applications perspective, the FE/magnetic heterostructures could become even superior to the currently available bulk multiferroics with regards to their magnetoelectric performance.[5–7] In these heterostructures, it is easier to obtain large FE polarizations and a robust magnetization, and the manifestations of the magnetoelectric coupling can be fairly diverse. For example, an exchange bias effect that can be controlled with electric fields has been recently reported in $La_{0.7}Sr_{0.3}MnO_3/BiFeO_3$,[8,9] and the associated physical mechanism that produces this interesting behavior is being actively discussed.[10–13]

Even without the magnetic coupling across the interface, interfacial magnetoelectric effects still generally exist in these heterostructures. A mechanism contributing to these effects involves the possibility of lattice distortions, since the oxides magnetic or FE properties are often sensitive to strain.[14–16] An additional contribution is the carrier-mediated field effect,[17,18] especially crucial in ultrathin film heterostructures. The FE field effect not only generates magnetoelectricity, but also gives rise to a bipolar resistive switching.[19–31]

A heterostructure FE field-effect transistor (FE-FET) is basically composed of a FE oxide film and a thin metallic or semiconducting oxide film, as sketched in Fig. 1, similarly to traditional FETs used in the semiconductor industry. In those standard FET devices, the conductivity of the semiconducting channel can be switched on and off by tuning the gate voltage. The FE-FETs can provide similar functions by switching the direction of the polarization of the FE gate. Moreover, this switching, at least ideally, can be nonvolatile due to the remnant FE polarization.[19,21] Furthermore, due to the strongly correlated character of the electronic component in several oxides, the above mentioned switching in FE-FET is not limited to the conductivity, but it may also influence other physical quantities as well, such as the magnetization, orbital order, elastic distortions, etc. Therefore compared with traditional semiconductor FETs, the physics in FE-FETs can be richer, and potentially additional functionalities can be expected.

Although the FE-FETs have been experimentally studied for several years, only recently, theoretical investigations have been focused on this topic.[17,18,32–35] These recent theoretical studies have been based on the density functional theory (DFT). In fact, studies using model Hamiltonians including strongly correlated electronic effects, beyond the reach of DFT, and focusing on the basic aspects of the FE field effect in these oxide heterostructures are rare. An important technical problem in this context is how to take into account the contribution from the FE polarization on the physics of the microscopic model Hamiltonian representing the other components. In recent efforts by some of us, the FE polarization was modeled as an interfacial potential at the first layer of the conducting channel,[36] but this approximation must be refined to address the subtle energy balances between competing tendencies near the interface. Thus, for all these reasons, in this manuscript, the FE-FET structures will be revisited using model Hamiltonian techniques and applying new approximations to handle this problem. Our effort has the main merit of paving the way for the use of models for the study of FE-FET systems where one of the components has a strongly correlated electronic character that is difficult to study via *ab initio* methods.

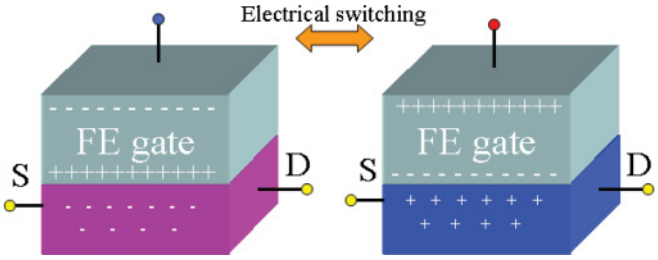

FIG. 1. (Color online) Sketch of an FE-FET heterostructure (S indicates the source and D the drain). The physical properties of the channel can be switched on and off by the FE polarization of the gate.

II. MODEL AND METHOD

A. Model Hamiltonian

As discussed in the introduction, in this manuscript, the FE field effect will be studied from the model Hamiltonian perspective. More specifically, here, the standard two-orbital (2O) double-exchange (DE) model will be used for the metallic component of the heterostructure. This 2O DE model is well known to be successful in modeling the perovskite manganites,[37–39] which are materials often used in FE-FET devices. Furthermore, previous model Hamiltonian studies have already confirmed that the 2O DE model, with some simple modifications, is still a proper model to use for manganite layers when they are in the geometry of a heterostructure.[36,40–44] In addition, since the DE mechanism provides a generic framework to describe the motion of electrons in several magnetic systems, the approach followed here, with minor modifications, could potentially be adapted to other oxides beyond the manganites.

As a widely accepted simplification, the limit of an infinite Hund coupling will be adopted in the DE model studied here. Then, more specifically, the model Hamiltonian of the metallic channel reads as

$$H = -\sum_{\langle ij\rangle}^{\gamma\gamma'} t_{\gamma\gamma'}^{\vec{r}}(\Omega_{ij} c_{i\gamma}^{\dagger} c_{j\gamma'} + \text{H.c.}) + \sum_i V_i n_i + \sum_{\langle ij\rangle} J_{\text{AF}} \vec{S}_i \cdot \vec{S}_j. \quad (1)$$

In this expression, the first term is the standard DE interaction. The operator $c_{i\gamma}$ ($c_{i\gamma}^{\dagger}$) annihilates (creates) an electron at the orbital γ of the e_g band and at the lattice site i, with its spin perfectly parallel to the localized t_{2g} spin $\vec{S}_i$. The indices i and j represent nearest-neighbor (NN) lattice sites. The Berry phase factor Ω_{ij}, generated by the infinite Hund coupling limit adopted here, equals $\cos(\theta_i/2)\cos(\theta_j/2) + \sin(\theta_i/2)\sin(\theta_j/2)\exp[-i(\phi_i - \phi_j)]$, where θ and ϕ are the polar and azimuthal angles defining the direction of the t_{2g} spins, respectively. When a ferromagnetic (FM) t_{2g} background is used, then $\Omega = 1$. The labels γ and γ' denote the two Mn e_g-orbitals a ($|x^2 - y^2\rangle$) and b ($|3z^2 - r^2\rangle$). The NN hopping direction is denoted by $\vec{r}$. The DE hopping depends on the direction in which the hopping occurs, and it is orbital-dependent as well. The actual hopping amplitudes are

$$t^x = \begin{pmatrix} t_{aa}^x & t_{ab}^x \\ t_{ba}^x & t_{bb}^x \end{pmatrix} = \frac{t_0}{4}\begin{pmatrix} 3 & -\sqrt{3} \\ -\sqrt{3} & 1 \end{pmatrix},$$
$$t^y = \begin{pmatrix} t_{aa}^y & t_{ab}^y \\ t_{ba}^y & t_{bb}^y \end{pmatrix} = \frac{t_0}{4}\begin{pmatrix} 3 & \sqrt{3} \\ \sqrt{3} & 1 \end{pmatrix},$$
$$t^z = \begin{pmatrix} t_{aa}^z & t_{ab}^z \\ t_{ba}^z & t_{bb}^z \end{pmatrix} = t_0\begin{pmatrix} 0 & 0 \\ 0 & 1 \end{pmatrix}, \quad (2)$$

where t_0 is the DE hopping amplitude scale. In the rest of this publication, t_0 is considered the unit of energy. Its real value is approximately 0.5 eV in wide-bandwidth manganites such as $La_{0.7}Sr_{0.3}MnO_3$ (LSMO).[37,38]

The second term in the Hamiltonian is the on-site potential energy: V_i is the actual potential at each site and n_i is the e_g electronic density operator at the same site. The last term is the Heisenberg-type antiferromagnetic (AFM) superexchange (SE) interaction between the localized NN t_{2g} spins. Its actual typical strength is about 10% that of t_0.[37,38]

B. Self-consistent calculations

In the actual calculations described in this publication, a cuboid lattice ($L_x \times L_y \times L_z$, $L_x = L_y = 4$, $L_z = 12$) will be used with open boundary conditions (OBCs) along the z axis to avoid having two interfaces.[36,42] Twisted boundary conditions (TBCs) are adopted in the x-y plane to reduce finite size effects via a 6×6 k mesh.

The FE gate will be here modeled as a surface charge (Q per site, in units of the elementary charge e, and located at $z = 0$) coupled to the first channel layer ($z = 1$). This approximation has been successfully confirmed in previous DFT calculations.[17,18,32–35] The long-range Coulomb interaction is included via a layer-dependent potential $V(z)$,[34] and within each layer the potential is assumed to be uniform for simplicity. This electrostatic potential is determined via the Poisson equation.[36,41–44] In particular, the electric field between the zth and $(z+1)$th layers is determined by the net charge $[Q + \sum_l^{1\leqslant l\leqslant z}(-n(l) + n_b)]$ counted from the FE interface, where $n(l)$ is the e_g electronic density corresponding to the lth layer, and n_b is the background (positive) charge density. Thus the electrostatic potential (with respect to the negative charge of electrons) of each layer can be calculated via the relation:

$$V(z+1) = V(z) + \alpha\left[Q + \sum_l^{1\leqslant l\leqslant z}[-n(l) + n_b)\right], \quad (3)$$

where α is the Coulomb coefficient, which is inversely proportion to the dielectric constant ε [$\alpha = c/(\varepsilon t_0)$, where c is the lattice constant, ε is the dielectric constant, and t_0 is in unit of eVs as explained before]. In the following, n_b is fixed at the value 0.7 since typical manganites are FM metals at this doping value, e.g., LSMO and $La_{0.7}Ca_{0.3}MnO_3$ (LCMO).[45]

In our computational study, the 12th layer is assumed to be sufficiently far from the interface such that V ($z = 12$) is set to be zero as the reference point of the electrostatic potential. This choice, combined with a fixed chemical potential, restores the system to its original bulk state for layers far from the

interface. A FM t_{2g} background is adopted to simulate the metallic channel in the FE-FET device. The DE Hamiltonian (including the term with $V_i n_i$) is diagonalized to obtain the charge distribution $n(z)$, which is iterated together with $V(z)$ until a self-consistent solution is reached. After convergence in $n(z)$ and $V(z)$, the total grand potential (per unit cell) can be calculated as

$$\Omega = \Omega_f - \frac{1}{2L_z}\sum_{z}^{1\leqslant z\leqslant L_z} V(z)n(z) - \frac{1}{2L_z}n_b\sum_{z}^{1\leqslant z\leqslant L_z} V(z) - \frac{1}{2L_z}V(0)Q + \frac{J_{\rm AF}}{L_xL_yL_z}\sum_{\langle i,j\rangle}\vec{S}_i\cdot\vec{S}_j, \quad (4)$$

where Ω_f is the fermionic grand potential (per site), calculated from the diagonalization eigenvalues. The second term considers the reduction of the electrostatic Coulomb energy of the e_g electrons, since it is doubly-counted in the first term. The third and fourth terms are the electrostatic Coulombic energies of the positive background charge (n_b) and the FE surface charge, respectively. The last term describes the AFM SE energy, namely, the Heisenberg interaction among the localized spins. A finite but low temperature $T = 0.005t_0$ (~30 K) is used for the Fermi-Dirac distribution function smearing.

III. RESULTS AND DISCUSSION

A. Charge accumulation/depletion

To investigate the screening effects in the FE-FET heterostructure, the results for four values of α (0.5, 1, 2, and 4) were compared. For each α, the surface charge Q is initially set to zero to find the chemical potential where the average e_g density equals n_b. With this chemical potential, Q is then varied from $+0.4$ to -0.4 (in units of the elementary charge per cell). Ideally, $|Q| = 0.4$ corresponds to a FE polarization as large as 40 μC/cm^2 (if the pseudocubic lattice constant c is set as 4 Å), which is a typical and reasonable value for standard FE oxide materials.

The screening effects correspond to the accumulation/depletion of charges near the interface. Under a positive (negative) Q, more e_g electrons will be attracted to (repelled from) the interface. Since the chemical potential is fixed in our simulation, the screening effect can also be obtained from the average e_g density as a function of Q, as shown in Fig. 2. This screening effect increases when α is increased, which is concomitant with a stronger electrostatic Coulomb interaction near the interface. In the rest of the manuscript, $\alpha = 2$ will be here adopted: using $t_0 = 0.5$ eV and $c = 4$ Å, this α value corresponds to a relative permittivity $\varepsilon_r \approx 45$, which is quite reasonable to represent real materials. Also note that $\alpha = 2$ is already very close to the fully screened case according to the results shown before. It should be remarked that the total charge for the whole system is zero (i.e., the combined FE gate and manganite channel are neutral) although the gate and channel themselves are charge polarized.

The screening effect is better observed by studying the e_g electron density profiles and their corresponding electrostatic potentials in Fig. 3. The $Q = +0.4$ and -0.4 cases are shown together for better comparison. When $Q = +0.4$, then

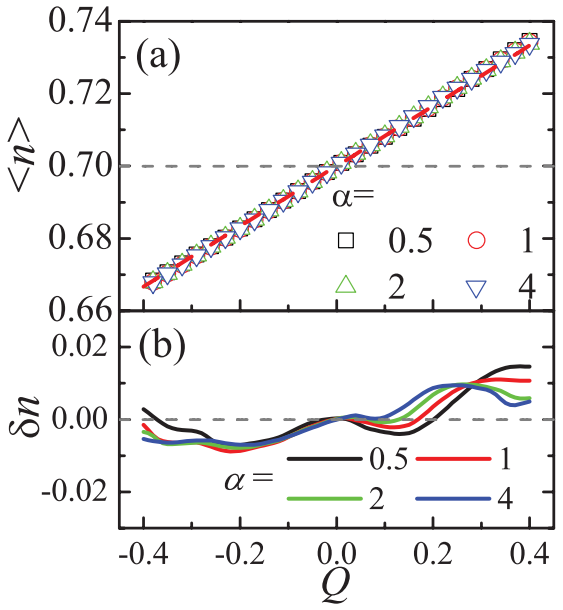

FIG. 2. (Color online) (a) The average e_g density $\langle n\rangle$ vs Q. The (red) dashed line corresponds to the fully screened case, where $\langle n\rangle = n_b + Q/L_z$. Here, only the electronic screening is considered, while the ionic screening[46] is neglected, since its effect can be partially expressed by the dielectric constant that enters in α and an effective Q. (b) The deviations of the e_g density from the fully screened limit, where $\delta n = (\langle n_i\rangle - n_b)\times L_z - Q$. The maximum deviation ($|\delta n|$) is <0.015 for $\alpha = 0.5$, which decreases to <0.01 for $\alpha = 2$ and 4.

$V(z)$ becomes deep enough near the interface to accumulate considerably more e_g electrons than in the bulk. In contrast, when $Q = -0.4$, then $V(z)$ is large and positive near the interface, thus repelling those e_g electrons. With $\alpha = 2$, the screening of e_g electrons is the most significant within a thin region near the interface, typically involving just 2–3 layers for the 2O DE model employed here.

B. Interfacial phase transitions

Since the previous results show that the interfacial electronic density can be substantially modulated by the FE polarization, then it is natural to expect local phase transitions. The reason is that the phase diagrams of oxides are usually

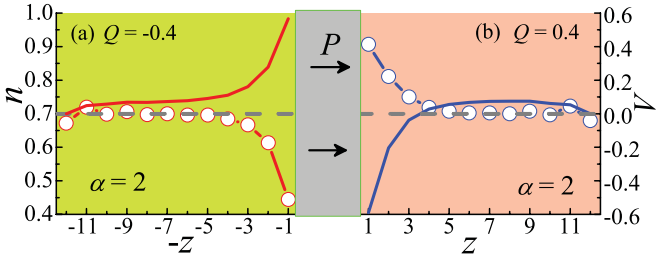

FIG. 3. (Color online) The e_g density profiles $n(z)$ (dots) and the electrostatic potential $V(z)$ (lines without dots). The cases $Q = -0.4$ (left) and $Q = 0.4$ (right) are shown together for better comparison. The FE gate is in the middle and its polarization points to the right as indicated. The original e_g density ($n_b = 0.7$) is shown as dashed lines for better reference.

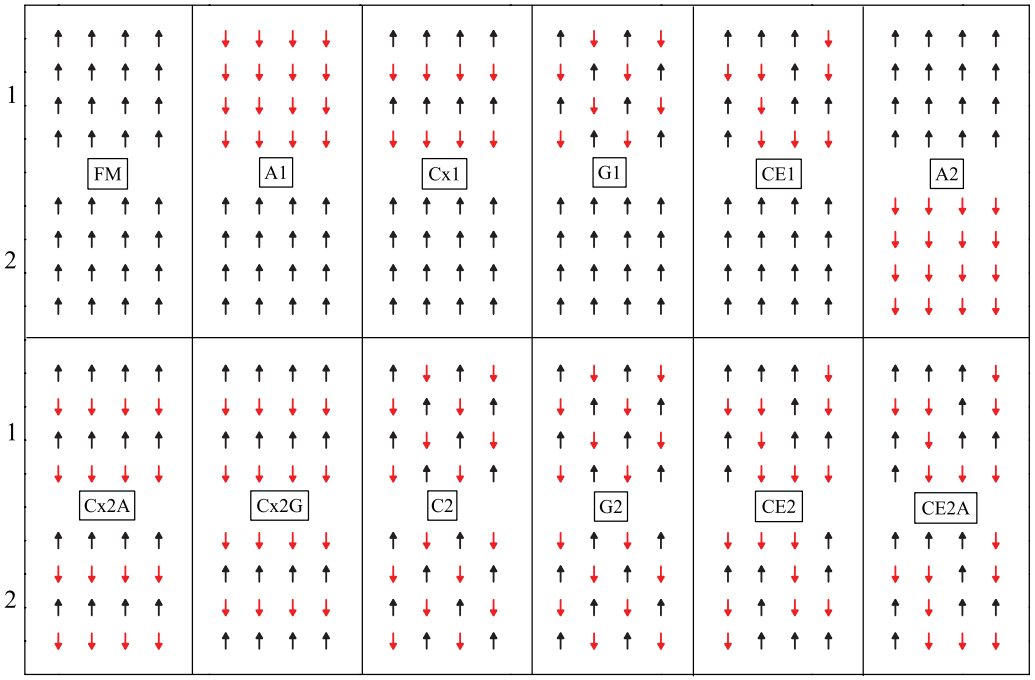

FIG. 4. (Color online) The candidates for the spin order at the two interfacial layers, as described in the main text. The layer indices (1 and 2) counting from the interface are shown on the left side of the figure. The FM spin order is the original one, in the absence of the surface charge Q. In the rest of the panels, the spins pointing down are shown in red. All spins in other layers ($z > 2$) point "up" for these variational states. Here, the choices for the spin candidate states are not arbitrary but have clear correspondences to states already known to exist in the bulk phase diagrams. In addition, some combinations of different magnetic orders in the two layers have also been included since the interfacial region may be different from the bulk.

highly sensitive to charge density variations,[47] i.e., density-driven phase transitions are well known to occur in bulk materials when chemically doped to modify the electronic density.[32,33] To explore these possible phase transitions, the zero-temperature variational method is here employed by comparing the total ground-state energy [Eq. (4)] for a variety of spin patterns. From Fig. 3, it is clear that most of the charge accumulation/depletion occurs within the first two layers near the FE interface. Hence, for simplicity, the several non-FM (collinear) spin patterns explored here will only be proposed to exist in these two layers in our present variational calculation, while the spins in the other layers remain fixed to be FM. The candidate spin patterns in the two interfacial layers are shown in Fig. 4.

The ground-state phase diagram obtained in our calculations for the interfacial layers in FE-FET is shown in Fig. 5. According to this phase diagram, the original FM metallic phase at $Q = 0$ is stable when $J_{AF} < 0.128$, while the boundary between the FM and A-type AFM phases is at $J_{AF} = 0.13$ for the calculation representing the bulk (see Fig. 7 later in this paper). These two, almost identical values suggest that the lattice size effects and surface effects are negligible in our simulation of FE-FET.

By adjusting the FE polarization (i.e., by modifying the surface charge Q) in the FE-FET setup, in the present variational effort it has been observed that the interfacial spins have a transition to arrangements different from the original FM state. This is the main result of our publication. For example, the CE1 and Cx1 orders are stabilized and replace the FM state in sequence with increasing negative Q when $J_{AF} \sim 0.12t_0$, as shown in Fig. 5. In contrast, the FM order remains robust under a positive Q, thus establishing an asymmetry in the response of the system to the FE polarization orientation that is of value for applications.

The FE screening effect plays an important role to determine the dominant interfacial spin order that is competing with the DE mechanism that favors ferromagnetism. Considering $J_{AF} = 0.12$ as example, when $Q < 0$, the CE1 and Cx1 orders can accommodate more holes near the interface than the original FM state, thus reducing the Coulomb potential pronouncedly, as shown in Fig. 6. In simple words, the

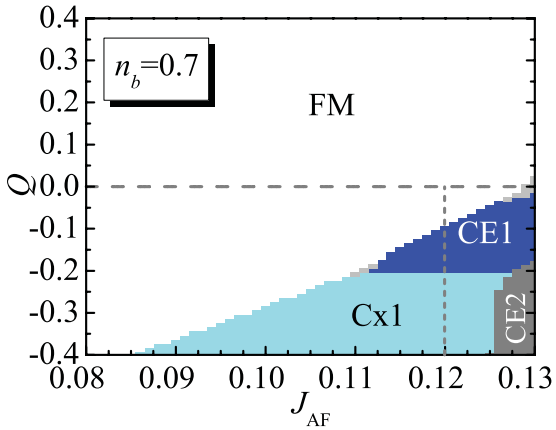

FIG. 5. (Color online) Ground-state phase diagram for the interfacial layers in FE-FET, obtained by the variational procedure described in the text.

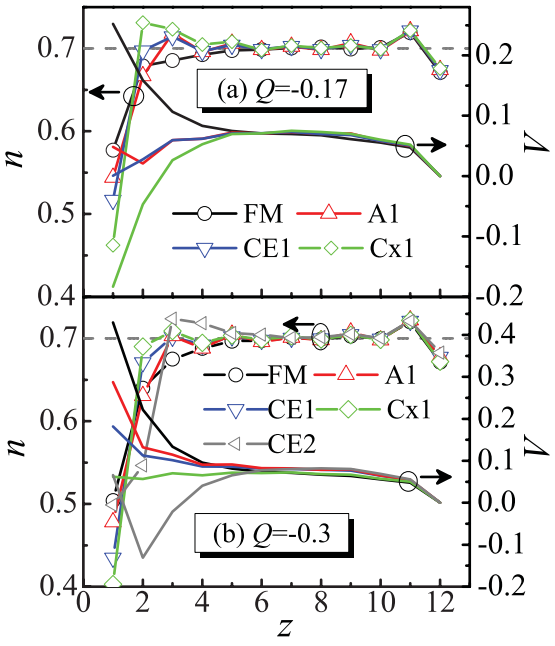

FIG. 6. (Color online) The e_g density profiles (left axes) and the corresponding electrostatic potentials (right axes) of the 2O model studied here. Panel (a) is for $Q = -0.17$, while panel (b) is for $Q = -0.3$. The ground states [CE1 state in (a) and Cx1 state in (b)] provide the best screening effect, i.e., a smooth potential $V(z)$ varying z.

system chooses an interfacial state which can screen the FE polarization rather well.

C. Comparison with bulk properties

For comparison, the ground state of the bulk is also calculated using the standard 2O DE model, under a similar variational approximation with states now covering the whole system. This information can be used as a guide to explore the interfacial spin orders that may be of relevance in the FE-FET setup. The results are shown in Fig. 7. Considering

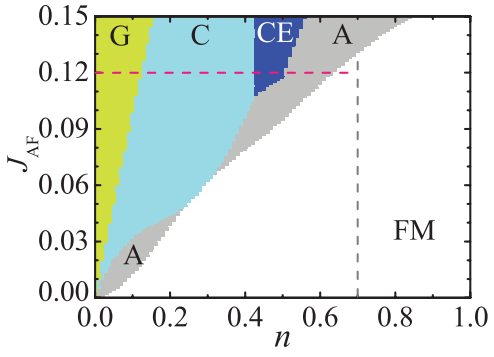

FIG. 7. (Color online) The ground-state phase diagram of the 2O DE model for manganites in the bulk, which is calculated using the variational method described in the text. All DE energies are obtained from analytical band structures. The phase boundary between the FM and A states at $n = 0.7$ is illustrated by the vertical dashed line, while the horizontal dashed line shows the phase transition at $J_{AF} = 0.12$ obtained by changing the e_g electron density. A, C, CE, and G denote the typical AFM phases found in manganites.[45]

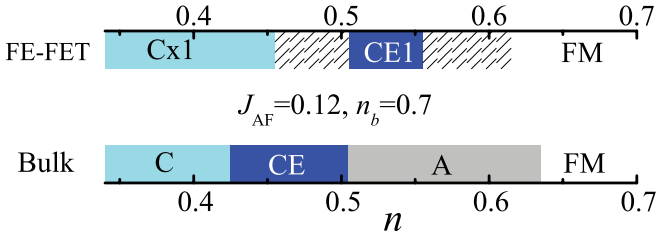

FIG. 8. (Color online) Comparison of the transitions found in the FE-FET heterostructure and in the bulk, at $J_{AF} = 0.12$. According to the bulk phase diagram, with decreasing electronic density, the bulk system turns from the FM phase into an A-type AFM state, followed by a CE phase and then by a C-type AFM state. However, in the FE-FET setup, from the original FM phase and with increasing $|Q|$, the spins in the first interfacial layer directly jump to the CE order, and then to the Cx1 order. Moreover, the shaded regions were found to be unstable due to phase separation tendencies in the FE-FET case.

the simplicity of the model (with only two competing NN interactions: DE versus SE), this phase diagram agrees fairly well with the experimental perovskite manganite results.[45] The most typical phases found in bulk manganites, namely, the FM and various AFM states (A, C, G, and CE types), appear in the proper e_g density and bandwidth regions, providing support to the qualitative accuracy of our calculations.

Considering $J_{AF} = 0.12$ as an example, Fig. 8 compares the spin-order transitions in the bulk and in the FE-FET. In the bulk's phase diagram, by reducing the e_g density from $n = 0.7$, the system transitions from a FM phase to an A-type AFM state at $n = 0.63$, then from A to CE at $n = 0.5$, and from CE to C-type AFM one at $n = 0.42$. In the FE heterostructure, on the other hand, the system changes from FM to CE1 at $Q = -0.1$ ($n = 0.62$ in FM and $n = 0.55$ in CE1), and then from CE1 to Cx1 at $Q = -0.19$ ($n = 0.51$ in CE1 and $n = 0.45$ in Cx1). There are several interesting aspects in this interfacial phase transitions. First, the "critical" e_g densities are found to be different between the bulk and the FE-FET heterostructure. Second, the fragile A-type AFM state is absent in the heterostructure geometry. Third, in the heterostructure the interfacial electronic density jumps at the locations of the spin-order transitions, causing some density regions to be unreachable (i.e., they are unstable). Such density discontinuities originate from the well-known electronic phase separation tendencies in manganites,[37–39] a phenomenon that does not have an analog in semiconducting devices. Last but not least, the CE1 and Cx1 states predicted here have not been considered in previous DFT studies, since these states typically need larger in-plane cells than previously analyzed with DFT. These two interfacial states, CE1 and Cx1, may exist particularly in those manganite channels with relative narrow bandwidths, such as LCMO.

There are two main reasons for the differences observed here in the phase diagrams between the bulk and the heterostructures. The first reason is the FE screening effect, as shown in Fig. 6, namely, the ground state near the interface is determined not only by the competition between the DE kinetic energy and the SE energy as in the bulk, but also by the electrostatic potential energy. Second, since the spin-order transitions occur only near the interface, the global phases shown here, except for the FM one, are actually "artificial"

phase-separated states involving a combination of the bulk and the interfacial states, a combination that may be more stable than the homogeneous spin orders in the FE-FETs. Thus these examples show that it is not enough to simply guess the interfacial spin orders from those in the bulk phase diagrams with only homogeneous phases: new states may emerge at the interfaces.

Furthermore, it should be noted that these phase transitions may be even more complex than our calculations suggest. For instance, other states beyond the candidates considered here, for instance, involving canted spins and thicker interfacial layers, may become stable in some regions. To reveal additional details of these interfacial phase transitions, unbiased (and very CPU time consuming) studies involving Monte Carlo simulations should be performed in the future, including electron-phonon couplings and finite-temperature effects. However, the results discussed here are already sufficient to clearly show that the original FM phase is indeed unstable toward other phases at the interface with an FE, which was the main goal of this publication.

D. Spin flip versus spin rotation

Although the studies described above already clearly show that interfacial phase transitions away from the FM state will occur by tuning the FE polarization, the fine details of these phase transitions remain unclear. Do these spins flip abruptly from one configuration to the other or do they rotate gradually upon increasing $|Q|$? Are there any canted spin-states tendencies besides the collinear spin candidates considered here? Reaching a full answer to these questions is computationally very difficult at the current state of typical Monte Carlo simulations with an effort that grows like the fourth power of the number of sites N. However, some studies concerning spin rotation versus- spin flip tendencies can still be carried out in a variational manner, as described below.

As shown in Fig. 5, the FM order turns into the CE1 order upon increasing $|Q|$, which involves only one interfacial layers. During this transition, half of the spins in the first layer flip to "down" spins in the final CE1 state. For simplicity, let us assume that this phase transition (spin flip) occurs via an in-plane spin rotation. To reach the CE1 order, the spins in the first layers are partitioned into CE type zigzag chains. Half of those zigzag chains are assumed to rotate synchronously, namely, they are characterized by a unique spin angle $\delta\theta$. Using the variational method, $\delta\theta$ can be determined as a function of Q, as shown in Fig. 9. Since the phase boundary between the FM and CE1 states also depends on the SE coupling (J_{AF}), the spin flip/rotation process varies with J_{AF}. For all nine sets of J_{AF} shown here, the "speeds" of the spin rotations are not uniform. Note that a sharp jump of $\delta\theta$ always exists in each of the curves. There are only a few spin canted states that are stable as intermediate states during the spin rotation process, most of which exist near the FM side (i.e., $\delta\theta \sim 0$). Thus, the spin canting process does not seem to be very robust, at least according to our qualitative calculations. Instead, a sudden spin flip may be the preferred process for the interfacial phase transitions.

A better characterization of the spin flip versus spin rotation tendencies relates with the first-order versus second-order

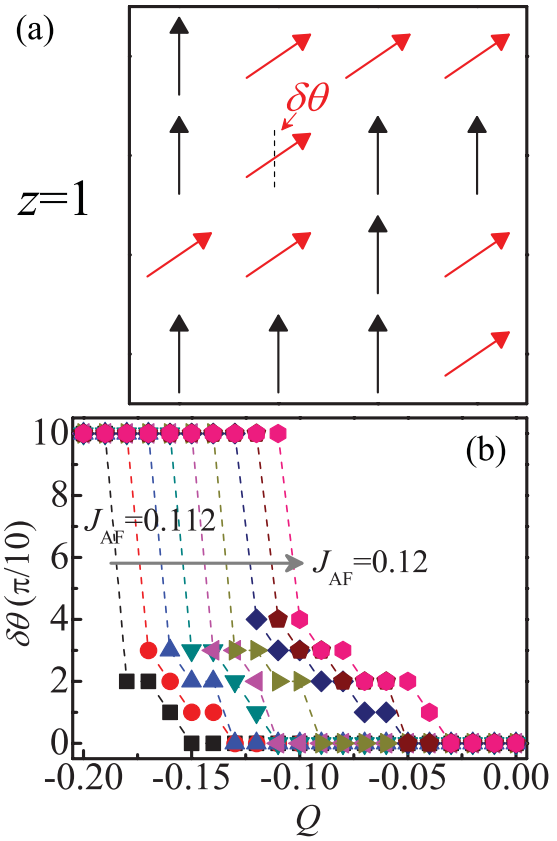

FIG. 9. (Color online) Possible spin flip/rotation process from the FM state ($\delta\theta = 0$) to the CE1 state ($\delta\theta = \pi$) during the interfacial phase transitions discussed before. (a) Sketch of the angle $\delta\theta$ used in the calculation. (b) Results for the nine sets of J_{AF} values (0.112–0.12) considered here.

transition character of the process. From Fig. 9, it seems that both spin flip and spin rotation are allowed. However, the canting angles $\delta\theta$'s are restricted near 0 in the spin flip case. Thus, there seems to occur a first-order transition between a FM-like (with $\delta\theta \sim 0$) and an AFM state (with $\delta\theta \sim \pi$). Of course, more powerful unbiased computational methods should be used to confirm this conclusion.

E. Resistive switching

Although the charge accumulation/depletion and associated local phase transitions induced by the switch of the FE polarization orientation occur only near the interface, these transitions lead to a global change in the conductance of the metallic channel (e.g., LSMO) when the FE polarization is flipped. This resistive switch effect should be bipolar, due to the asymmetric phase diagram found in our calculations, as shown in Fig. 5. This effect should also be anisotropic, because in a metallic channel, when the interfacial layers become less conducting due to the previously described phase transitions, the out-of-plane conductance will be seriously suppressed basically due to the spin valve effect,[33,35] while the in-plane transport will be only weakly affected, as shown in Fig. 10. It should be noted that here a good FM metallic channel is used, while more prominent resistive changes are expected

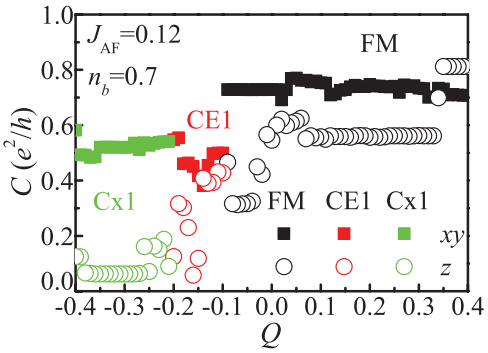

FIG. 10. (Color online) The Kubo conductance as a function of Q.[48] Both the in-plane (xy) and out-of-plane (z) conductances are shown.

to occur in those systems which are close to metal-insulator phase boundaries.

Besides the changes of the resistivity, magnetoelectric effects have also been observed in experimentally studied FE-FET heterostructures.[22–24] Qualitatively, the change of the magnetization can be understood via the local phase transitions near the interface when the FE polarization is flipped (see Figs. 6 and 9), as described in this manuscript.

Finally, it should also be noted that our current effort provides just a starting point to study the FE field-effect heterostructures with the use of model Hamiltonians. Additional realistic effects in real heterostructures were neglected in the present work, such as lattice structural distortions and chemical bonding effects. Thus the current predictions may be not as accurate as those reached with DFT calculations for some particular materials. The main relevance of the present model-based study is that it can provide overall tendencies for a material family. The study of the effect of more realistic interactions and the inclusion of finite-temperature effects can be achieved in future calculations based on the model described here.

IV. CONCLUSIONS

In summary, a microscopic model Hamiltonian for the FE oxide—FM metallic oxide heterostructures—a prototypical FE-FET system, has been studied here. The FE field effect is modeled via the electrostatic Coulomb potential in the FM oxide. Using a self-consistent calculation and the variational method, an interfacial charge accumulation/depletion is found by tuning the magnitude and sign of the FE polarization. Phase transitions at the interface have been observed here by modulating the electronic charge density of the metallic component by varying the FE polarization. Our present effort provides a starting point to study the FE field effect via model Hamiltonians. Our results clearly present some common similarities with previous DFT effort, confirming their main results. However, the framework is conceptually different and the results reported here are not identical to those of DFT. Moreover, our model is generic and it can be adapted to study a variety of other oxide heterostructures involving ferroelectrics, particularly those where the metallic component has a strongly correlated electronic character.

ACKNOWLEDGMENTS

We thank Ho Nyung Lee and Evgeny Tsymbal for helpful discussions. S.D. and J.M.L were supported by the 973 Projects of China (2011CB922101, 2009CB623303), NSFC (11004027), and NCET (10-0325). R.Y. was supported by the NSF Grant (DMR-1006985) and the Robert A. Welch Foundation (C-1411). X.Z. and E.D. were supported by the US Department of Energy, Office of Basic Energy Sciences, Materials Sciences and Engineering Division.

[1] E. Dagotto, Science **318**, 1076 (2007).
[2] H. Takagi and H. Y. Hwang, Science **327**, 1601 (2010).
[3] J. Mannhart and D. G. Schlom, Science **327**, 1607 (2010).
[4] G. Hammerl and N. Spaldin, Science **332**, 922 (2011).
[5] R. Ramesh and N. A. Spaldin, Nat. Mater. **6**, 21 (2007).
[6] M. Bibes, J. E. Villegas, and A. Barthélémy, Adv. Phys. **60**, 5 (2011).
[7] C.-W. Nan, M. I. Bichurin, S. X. Dong, D. Viehland, and G. Srinivasan, J. Appl. Phys. **103**, 031101 (2008).
[8] S. W. Wu, S. A. Cybart, P. Yu, M. D. Rossell, J. X. Zhang, R. Ramesh, and R. C. Dynes, Nat. Mater. **9**, 756 (2010).
[9] P. Yu, J.-S. Lee, S. Okamoto, M. D. Rossell, M. Huijben, C.-H. Yang, Q. He, J. X. Zhang, S. Y. Yang, M. J. Lee, Q. M. Ramasse, R. Erni, Y.-H. Chu, D. A. Arena, C.-C. Kao, L. Martin, and R. Ramesh, Phys. Rev. Lett. **105**, 027201 (2010).
[10] S. Dong, K. Yamauchi, S. Yunoki, R. Yu, S. Liang, A. Moreo, J.-M. Liu, S. Picozzi, and E. Dagotto, Phys. Rev. Lett. **103**, 127201 (2009).
[11] K. D. Belashchenko, Phys. Rev. Lett. **105**, 147204 (2010).
[12] K. L. Livesey, Phys. Rev. B **82**, 064408 (2010).
[13] S. Okamoto, Phys. Rev. B **82**, 024427 (2010).
[14] R. K. Zheng, J. Wang, X. Y. Zhou, Y. Wang, H. L. W. Chan, C. L. Choy, and H. S. Luo, J. Appl. Phys. **99**, 123714 (2006).
[15] R. K. Zheng, H.-U. Habermeier, H. L. W. Chan, C. L. Choy, and H. S. Luo, Phys. Rev. B **80**, 104433 (2009).
[16] E. J. Guo, J. Gao, and H. B. Lu, Appl. Phys. Lett. **98**, 081903 (2011).
[17] J. M. Rondinelli, M. Stengel, and N. A. Spaldin, Nat. Nano. **3**, 46 (2008).
[18] C.-G. Duan, J. P. Velev, R. F. Sabirianov, Z. Zhu, J. Chu, S. S. Jaswal, and E. Y. Tsymbal, Phys. Rev. Lett. **101**, 137201 (2008).
[19] C. H. Ahn, J.-M. Triscone, N. Archibald, M. Decroux, R. H. Hammond, T. H. Geballe, Ø. Fischer, and M. R. Beasley, Science **269**, 373 (1995).
[20] S. Mathews, R. Ramesh, T. Venkatesan, and J. Benedetto, Science **276**, 238 (1997).
[21] J. Hoffman, X. Pan, J. W. Reiner, F. J. Walker, J. P. Han, C. H. Ahn, and T. P. Ma, Adv. Mater. **22**, 2957 (2010).
[22] H. J. A. Molegraaf, J. Hoffman, C. A. F. Vaz, S. Gariglio, D. van der Marel, C. H. Ahn, and J.-M. Triscone, Adv. Mater. **21**, 3470 (2009).

[23]C. A. F. Vaz, J. Hoffman, Y. Segal, J. W. Reiner, R. D. Grober, Z. Zhang, C. H. Ahn, and F. J. Walker, Phys. Rev. Lett. **104**, 127202 (2010).
[24]C. A. F. Vaz, Y. Segal, J. Hoffman, R. D. Grober, F. J. Walker, and C. H. Ahn, Appl. Phys. Lett. **97**, 042506 (2010).
[25]X. Hong, A. Posadas, and C. H. Ahn, Appl. Phys. Lett. **86**, 142501 (2005).
[26]T. Zhao, S. B. Ogale, S. R. Shinde, R. Ramesh, R. Droopad, J. Yu, K. Eisenbeiser, and J. Misewich, Appl. Phys. Lett. **84**, 750 (2004).
[27]C. Thiele, K. Dörr, L. Schultz, E. Beyreuther, and W.-M. Lin, Appl. Phys. Lett. **87**, 162512 (2005).
[28]A. R. Chaudhuri, R. Ranjith, S. B. Krupanidhi, R. V. K. Mangalam, and A. Sundaresan, Appl. Phys. Lett. **90**, 122902 (2007).
[29]Y. Watanabe, Appl. Phys. Lett. **66**, 1770 (1995).
[30]O. Kuffer, I. Maggio-Aprile, and Ø. Fischer, Nat. Mater. **4**, 378 (2005).
[31]M. Eblen-Zayas, A. Bhattacharya, N. E. Staley, A. L. Kobrinskii, and A. M. Goldman, Phys. Rev. Lett. **94**, 037204 (2005).
[32]J. D. Burton and E. Y. Tsymbal, Phys. Rev. B **80**, 174406 (2009).
[33]J. D. Burton and E. Y. Tsymbal, Phys. Rev. Lett. **106**, 157203 (2011).
[34]M. Stengel, Phys. Rev. Lett. **106**, 136803 (2011).
[35]N. C. Bristowe, M. Stengel, P. B. Littlewood, J. M. Pruneda, and E. Artacho, e-print arXiv:1108.2208 (unpublished).
[36]M. J. Calderón, S. Liang, R. Yu, J. Salafranca, S. Dong, S. Yunoki, A. Moreo, and E. Dagotto, Phys. Rev. B **84**, 024422 (2011).
[37]E. Dagotto, T. Hotta, and A. Moreo, Phys. Rep. **344**, 1 (2001).
[38]E. Dagotto, *Nanoscale Phase Separation and Colossal Magnetoresistance* (Springer, Berlin, 2002).
[39]E. Dagotto, New J. Phys. **7**, 67 (2005).
[40]S. Dong, R. Yu, S. Yunoki, G. Alvarez, J.-M. Liu, and E. Dagotto, Phys. Rev. B **78**, 201102(R) (2008).
[41]L. Brey, Phys. Rev. B **75**, 104423 (2007).
[42]R. Yu, S. Yunoki, S. Dong, and E. Dagotto, Phys. Rev. B **80**, 125115 (2009).
[43]M. J. Calderón, J. Salafranca, and L. Brey, Phys. Rev. B **78**, 024415 (2008).
[44]B. R. K. Nanda and S. Satpathy, Phys. Rev. B **78**, 054427 (2008).
[45]Y. Tokura, Rep. Prog. Phys. **69**, 797 (2006).
[46]M. F. Chisholm, W. Luo, M. P. Oxley, S. T. Pantelides, and H. N. Lee, Phys. Rev. Lett. **105**, 197602 (2010).
[47]E. Dagotto, Science **309**, 257 (2005).
[48]J. A. Vergés, Comput. Phys. Commun. **118**, 71 (1999).